

Received 13 September 2022, accepted 6 October 2022, date of publication 12 October 2022, date of current version 19 October 2022.

Digital Object Identifier 10.1109/ACCESS.2022.3213939

RESEARCH ARTICLE

Direct Power Control Based on Point of Common Coupling Voltage Modulation for Grid-Tied AC Microgrid PV Inverter

SHAMEEM AHMAD^{1,2}, UMME KULSUM JHUMA²,
MAZAHER KARIMI³, (Senior Member, IEEE), ALIREZA POURDARYAEI^{4,5},
SAAD MEKHILEF^{2,6}, (Fellow, IEEE), HAZLIE MOKHLIS^{1,2}, (Senior Member, IEEE),
AND KIMMO KAUHANIEMI³, (Member, IEEE)

¹Department of Electrical and Electronics Engineering, Faculty of Engineering, American International University–Bangladesh (AIUB), Dhaka 1229, Bangladesh

²Department of Electrical Engineering, Universiti Malaya, Kuala Lumpur 50603, Malaysia

³School of Technology and Innovations, University of Vaasa, FI-65200 Vaasa, Finland

⁴Technical Planning and Load Forecasting Office, Hormozgan Regional Electric Company, Bandar Abbas 7916795599, Iran

⁵Department of Electrical and Computer Engineering, University of Hormozgan, Bandar Abbas 7916193145, Iran

⁶School of Science, Computing and Engineering Technologies, Swinburne University of Technology, Hawthorn, VIC 3122, Australia

Corresponding author: Mazaher Karimi (mazaher.karimi@uvasa.fi)

This research has been supported by the University of Vaasa under the Centralized Intelligent and Resilient Protection Schemes for Future Grids Applying 5G (CIRP-5G) research project funded by Business Finland with Grant No. 6937/31/2021. Some parts of this work were done in the SolarX research project funded by Business Finland with Grant No. 6844/31/2018.


ABSTRACT In this paper, a direct power control (DPC) approach is proposed for grid-tied AC MG's photovoltaic (PV) voltage source inverter (VSI) to regulate directly active and reactive powers by modulating microgrid's (MG) point of common coupling (PCC) voltage. The proposed PCC voltage modulated (PVM) theory-based DPC method (PVMT-DPC) is composed of nonlinear PVM, nonlinear damping, conventional feedforward, and feedback PI controllers. For grid synchronization rather than employing phase-locked-loop (PLL) technology, in this study, direct power calculation of the PCC voltage and current is adopted. Subsequently, at PCC, the computed real and reactive powers are compared with reference powers in order to generate the VSI's control signals using sinusoidal pulse width modulation (SPWM). Because of the absence of the PLL and DPC method adoption, the suggested controller has a faster convergence rate compared to traditional VSI power controllers. Additionally, it displays nearly zero steady-state power oscillations, which assures that MG's power quality is improved significantly. To validate the proposed PVMT-DPC method's performance real-time simulations are conducted via a real-time digital simulator (RTDS) for a variety of cases. The results demonstrate that PV VSI using the suggested PVMT-DPC approach can track the reference power quicker (0.055 s) along with very low steady-state power oscillations, and lower total harmonic distortion (THD) of 1.697% at VSI output current.

INDEX TERMS Direct power control, grid-tied, microgrid, PLL, power quality, RTDS, voltage source inverter control.

I. INTRODUCTION

In conventional power systems, fossil fuel resources are commonly employed to generate electricity, resulting in the rapid depletion of fossil fuels and increased pollution. Renewable energy is emerging as a viable alternative to address global

environmental and fossil fuel scarcity challenges. Thus, modern utility network has experienced significant transformations and upgrades to incorporate renewable sources of energy in the utility grid. This new technology is known as Microgrid (MG), which has used power electronic devices to connect non-dispatchable and dispatchable distributed generation (DG) units to the utility grid, ensuring communities have uninterrupted electricity. While MGs have numerous

The associate editor coordinating the review of this manuscript and approving it for publication was Ahmed F. Zobaa .

advantages such as low capital expense, a short return of investment period, and high reliability, with the association of their operation, more technical issues are still awaiting to be overcome, including during grid-tied mode operation, it is crucial to have an adaptable controller to maintain power flow between the main grid and MG. Meanwhile, during islanding operation, the system must have the ability to control the voltage magnitude and frequency [1]. The control method to manage the flow of power (real and reactive) between MG and power grid, for the effective operation of grid integrated AC MG consisting of various DGs has been put into consideration in this paper.

The major components of grid-tied MG are the voltage source inverters (VSI) which employ appropriate power control mechanisms to regulate power flow between MG & power grid and integrate renewable energy based DG units of MG into the grid. In the modern power grid, the penetration of renewable energy resources of MG is growing rapidly. Therefore, for grid-tied VSI, it is very crucial to maintain high power quality and stability. In the occurrence of drastic changes, the power controllers enable the MG system to respond quickly and have a lower rate of error for steady-state and to remain stable [1], [2]. The typical strategy for controlling the output power of grid-tied VSIs is to employ a rotating synchronous reference frame based trajectory current control theory (CCT) based method [1].

Numerous power control techniques based on dq CCT are developed in order to improve the efficacy, safety, and reliability of grid-connected MG VSIs. For the smooth operation of grid-connected AC MG VSI, in [1] a CCT based dq axes synchronous reference frame based power control approach is proposed. In [3], a power controller based on decoupled dq current control method has been developed and verified for grid integration of photovoltaic (PV) and battery storage in AC MG. The author in [4] proposes a firm power controller for a grid-connected VSI in order to increase the quality of the AC MG power. In [5], the latest artificial neural network (ANN)-based power control approach is proposed for managing the quality of PV-integrated AC MG power. In [6], real power, reactive power, and the voltage at the point of common coupling are used to design a control strategy for regulating power of VSI on grid-tied AC MG. A new power control strategy for an AC MG VSI is proposed in [7] in order to cascade voltage and current controllers. Power control method based on sliding mode is provided in [8] for a grid-linked PV/hydrogen integrated system. For a grid-tied MG, in [9] an optimal power flow control strategy is proposed based on a real-time self-tuning-based approach. In [10], a power control technique for a PV/Battery hybrid system integrated with the utility grid is presented. For grid-tied AC MGs with DG interfaced VSIs, a technique by coupling voltage support and harmonic compensation is provided in [11]. In [12], a control approach is devised in which the MG is connected to a distorted grid to improve power quality. In [13], a new control and power management technique was developed for a grid-connected MG.

Under partially shadowed conditions, an optimal power regulation for a grid-connected MG PV system is proposed in [14]. For all these mentioned control approaches, in order to guarantee that the dq axis grid voltages and currents are in phase with one another, phase angle of voltage is utilized in Park transformation during abc to dq conversion which must be appropriately retrieved from the grid [15]. PLL is the most frequently utilized technology for grid synchronization [16]. In order to derive the phase angle, grid voltages must be filtered and the arctangent function must be used [17]. Nevertheless, the PLL mechanism produces a delayed transient response. In [18], the detrimental effect of the PLL on the VSIs small-signal stability was documented. PLL systems also build massive power fluctuations in the real and reactive powers [19]. Additionally, PLL can degrade the stability of VSIs by generating negative resistance at low frequencies [20]. The frequency coupling dynamics of VSIs generated by the PLL were also fully demonstrated in [21] and [22]. The frequency range of the negative resistance is determined using the PLL's bandwidth. As a result, in addition to enhancing the stability and robustness of VSIs, a limited bandwidth PLL is typically used, compromising the system's dynamic performance greatly. To circumvent the PLL system's limitations, some studies [23], [24], [25] proposed frequency locked loop (FLL)-based synchronization solution for the MG's VSI [23], [24], [25]. Power control approach based on PLL-less CCT is introduced in [26] for grid-tied hybrid MG's VSI. Although power tracking performance of these control systems has improved marginally, there are still undesired ripples observed in both real and reactive powers.

Additionally, two feedback control loops have been adopted in the aforementioned controllers, namely the outer and inner control loops for power and current control, respectively which lead to the enhancement of the computation burden of the control methods [27]. To address this issue, the direct power control (DPC) approach for VSI is proposed, which does not require the use of an inner-loop current regulator. For example, a control mechanism to control real and reactive power has been presented based on DPC in [27] and [28]. Nonetheless, these approaches have variable switching frequencies, hence, building a line filter is problematic because the fluctuated switching frequency results in an unanticipated harmonic spectrum. A DPC technique based on model predictive control that takes into account system limits, nonlinearities, and multivariable samples is presented in [29] and [30]. Nevertheless, this strategy imposed an additional computational strain. Despite the fact that all of these solutions required only a single power control loop, PLL is still used for synchronization. Furthermore, because of the presence of multivariate parameters, these controllers operate poorly under changing dynamic load conditions, and no tests have been carried out to validate these controllers' performance for MG applications. For improving the power quality, few more new controllers have been proposed and tested for unbalanced grid conditions in [31], [32], and [33].

However, their applications are limited to an electric vehicle.

For a grid-connected MG's PV VSI mode grid, this paper aims to design a simple, robust and flexible DPC method based on PCC voltage modulated theory (PVMT) in order to improve not only transient responsiveness but also steady-state performance of MG's PV VSI, notably power oscillations. Additionally, feedforward decoupled control and feedback PI control method are employed in the PVMT-DPC approach incorporating a non-linear PCC voltage modulated (PVM) control. Since the proposed PVMT based DPC does not require any PLL system and Park transformation to create new control inputs in the dq frame, it has the advantage over traditional PLL-CCT based power controllers. As a result, as compared to the standard power controller based on PLL, the suggested power controller has a superior and faster dynamic and transient performance. Furthermore, the computational complexity is decreased because the proposed PVMT-DPC technique includes merely a single power control loop that directly manages the contemporaneous real and reactive power flow. Furthermore, the feedforward decoupled control has abolished the existence of coupling terms in the new control inputs, and finally, for the real and reactive power, feedback PI control technique is used to get two distinct dynamics of the 2nd order error signals. To ensure the rate of convergence of the real and reactive powers, the gains values of PI controllers are set using the phase margin and cutoff frequency of the entire MG system dynamics. During islanded mode of MG, the bus voltage and frequency are governed by a voltage and frequency (V-f) control method from [34], while, a power management approach proposed in [1] is used to maintain appropriate power flow among various energy sources and loads in the AC MG.

For grid synchronization in this study, instead of employing park transformation and PLL system, PVMT is employed where PCC voltage and current are used to provide direct power calculation. The DPC modeling for PV VSI is also broadly represented. The RSCAD platform is employed to model the electromagnetic transients of the AC MG. For the performance verification of the proposed PVMT-DPC approach, real-time simulations in a real-time digital simulator (RTDS) are conducted for testing purposes by changing real and reactive power references. Proposed PVMT-DPC method performance is also verified during MG's different operating modes (islanded & grid-tied) by varying MGs load and PV's solar irradiation simultaneously. In this study, real-time simulations of several grid-connected MG power control systems are carried out, and their performances are compared to those of the PVMT-DPC approach.

The rest of the paper is organized as: The configuration of the proposed AC MG is presented in section II. VSI based on PVMT is discussed in Section III, which includes mathematical modeling. Section IV illustrates the design of the suggested DPC strategy. The findings of the real-time simulations were reported in Section V, together with a full

TABLE 1. AC MG parameters.

| Parameters | Value |
|--|-----------------------|
| 0.1 MW PV System | |
| Series connected PV modules | 28 |
| PV module Temperature | 25 °C |
| Parallel connected PV modules | 68 |
| Reference PV irradiation | 1000 W/m ² |
| Maximum power voltage | 17.3 V |
| Voltage at open circuit | 21.5 V |
| Maximum power current | 3.05 A |
| Current during short circuit | 3.33 A |
| PV VSI | |
| DC-link voltage | 975 V |
| Switching frequency PV Inverter | 2 kHz |
| Capacitor for DC link | 500 uF |
| Inductance of Filter | 5.5 mH |
| Resistance of Filter | 0.001 Ω |
| 15 kWh Battery Storage System | |
| Series connected cells | 135 |
| Parallel connected cells | 290 |
| Battery SOC | Greater than 85% |
| Capacity per cell | 0.85 AH |
| Nominal voltage per cell | 3.6 V |
| Battery VSI | |
| DC-link voltage | 975 V |
| Switching frequency battery Inverter | 2 kHz |
| DC link capacitor | 450 uF |
| Inductance of Filter | 6 mH |
| Resistance of Filter | 0.01 Ω |
| Grid | |
| Rated voltage | 13.2 kV |
| Grid frequency | 60 Hz |
| Primary/Secondary voltage of Transformer | 0.48 kV/13.2 kV |
| 0.20 MVA Diesel Generator | |
| Voltage rated | 0.48 kV |
| Rated power | 0.20 MVA |
| Load | |
| Non-critical | 0.05-0.2 MW |
| Critical | 0.05 MW |
| Buck-Boost Converter | |
| Inductance | 6 mH |
| Switching frequency | 20 kHz |
| Boost Converter | |
| Switching frequency | 20 kHz |
| Inductance | 8 mH |
| Capacitance | 85 uF |

discussion and comparison result with the existing technique. Finally, section VI concludes the work.

II. TESTBED OF AC MICROGRID

The schematic of the testbed of the grid-connected AC MG adopted in this study is represented in Fig. 1, which is consisted of a battery storage system, a PV system and a diesel generator.

By using the available modules from RSCAD library for various MG components, the AC MG is modeled and these components mathematical modeling adopted from [26]. The specifications of all the MG components are presented in Table 1. Two VSIs are used to integrate the MG's battery and PV systems through a 3-ph transformer with the grid. During grid failure to provide emergency backup a diesel

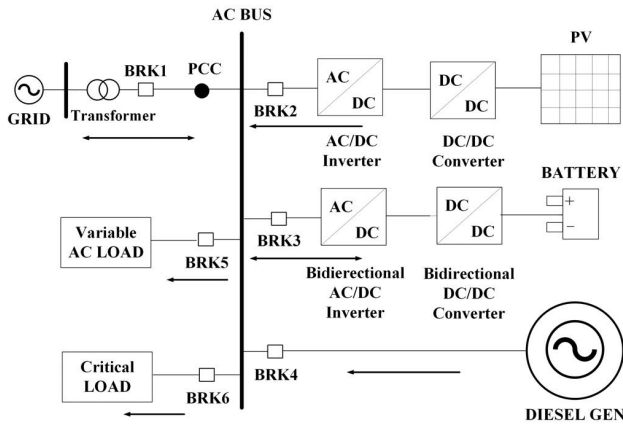


FIGURE 1. AC microgrid testbed schematic.

generator is used and loads of two types are considered namely non-critical and critical loads where critical load gets uninterrupted power supply.

III. PCC VOLTAGE MODULATED VSI MODELING

This section presents the mathematical modeling of PVMT based VSI. The PV system is connected to the DC-link of the PVMT-DPC based VSI through DC–DC boost converter where the output of the battery bidirectional DC-DC buck boost converter is connected to the DC link of PLL-CCT based VSI. Through L-filters PV and battery systems' VSIs are connected to the grid. The pictorial representation of the typical PLL-CCT based power control technique [1], and proposed PVMT-DPC method are presented in Fig. 2 (a) and (b) respectively which are explained in detail in later section.

The dynamic relation among VSI output voltages, PCC voltages, and VSI output currents can be represented as (1):

$$v_{abcg} = u_{abc} - Ri_{abc} - L \frac{di_{abc}}{dt} \quad (1)$$

where, output voltages of VSI, voltages at PCC and output currents of VSI are denoted by v_{abcg} , u_{abc} and i_{abc} , and respectively. L and R are the inductance and resistance of VSI output filter respectively.

Stationary reference model of (1) can be obtained as (2) through Clark transformation.

$$v_{\alpha\beta g} = u_{\alpha\beta} - Ri_{\alpha\beta} - L \frac{di_{\alpha\beta}}{dt} \quad (2)$$

where, $v_{\alpha\beta g}$, $i_{\alpha\beta}$ and $u_{\alpha\beta}$ represent PCC voltages, currents and voltages of VSI in $\alpha - \beta$ frame respectively.

The stationary model for instant real and reactive power model in $\alpha - \beta$ frame between grid and VSI can be represented as follows:

$$\begin{aligned} P &= \frac{3}{2} (i_{\alpha} v_{\alpha g} + i_{\beta} v_{\beta g}) \\ Q &= \frac{3}{2} (-i_{\beta} v_{\alpha g} + i_{\alpha} v_{\beta g}) \end{aligned} \quad (3)$$

where, P and Q denote instant real and reactive powers of grid respectively.

By differentiating (3), the equations of the powers in dynamic form are obtained as (4).

$$\begin{aligned} \frac{dP}{dt} &= \frac{3}{2} \left(v_{\alpha g} \frac{di_{\alpha}}{dt} + i_{\alpha} \frac{dv_{\alpha g}}{dt} + v_{\beta g} \frac{di_{\beta}}{dt} + i_{\beta} \frac{dv_{\beta g}}{dt} \right) \\ \frac{dQ}{dt} &= \frac{3}{2} \left(-v_{\alpha g} \frac{di_{\beta}}{dt} - i_{\beta} \frac{dv_{\alpha g}}{dt} + v_{\beta g} \frac{di_{\alpha}}{dt} + i_{\alpha} \frac{dv_{\beta g}}{dt} \right) \end{aligned} \quad (4)$$

Voltage relationship expressed in (5) can be used for simplifying dynamics of power presented in (4) due to balanced condition of the grid.

$$\begin{aligned} v_{\alpha g} &= V_{pcc} \cos(\omega t) \\ v_{\beta g} &= V_{pcc} \sin(\omega t) \end{aligned} \quad (5)$$

where,

$$V_{pcc} = \sqrt{v_{\alpha g}^2 + v_{\beta g}^2} \quad (6)$$

where, amplitude of PCC voltage amplitude is V_{pcc} , angular frequency, $\omega = 2\pi f$, and grid voltage frequency is f .

PCC voltages dynamic equations can be obtained as (7) by differentiating (5).

$$\begin{aligned} \frac{dv_{\alpha g}}{dt} &= -\omega V_{pcc} \sin(\omega t) = -v_{\beta g} \omega \\ \frac{dv_{\beta g}}{dt} &= \omega V_{pcc} \cos(\omega t) = v_{\alpha g} \omega \end{aligned} \quad (7)$$

By substituting (1) and (7) in (4), the dynamic real and reactive power equations can be obtained as (8).

$$\begin{aligned} \frac{dp}{dt} &= \frac{3}{2L} \left(-V_{pcc}^2 + u_{\alpha} v_{\alpha g} + u_{\beta} v_{\beta g} \right) - \omega q - p \frac{R}{L} \\ \frac{dq}{dt} &= \frac{3}{2L} \left(-u_{\beta} v_{\alpha g} + u_{\alpha} v_{\beta g} \right) - \omega q - q \frac{R}{L} \end{aligned} \quad (8)$$

New control inputs based on voltage modulation can be obtained as (9), by simplifying the real and reactive power dynamics expressed in (8) using theory of voltage modulation [28].

$$\begin{aligned} u_P &:= u_{\alpha} v_{\alpha g} + u_{\beta} v_{\beta g} \\ u_Q &:= u_{\beta} v_{\alpha g} - u_{\alpha} v_{\beta g} \end{aligned} \quad (9)$$

where, new voltage modulated control inputs are U_P and U_Q . These control inputs (U_P and U_Q) can be converted to DC components U_d and U_q respectively, as they satisfy (10).

$$\begin{aligned} \begin{bmatrix} u_P \\ u_Q \end{bmatrix} &= V_{pcc} \begin{bmatrix} \cos(\omega t) & \sin(\omega t) \\ -\sin(\omega t) & \cos(\omega t) \end{bmatrix} \begin{bmatrix} u_{\alpha} \\ u_{\beta} \end{bmatrix} \\ &= V_{pcc} \begin{bmatrix} u_d \\ u_q \end{bmatrix} \end{aligned} \quad (10)$$

where, dq voltages of the VSI are u_d and u_q respectively. Further, it can be seen from (10) that, without PLL system also the system can be represented in dq frame.

By substituting new control inputs (u_P and u_Q) obtained from (9) to (8), the real and reactive power dynamics in (8) can be expressed as (11).

$$\begin{aligned} \frac{dP}{dt} &= \frac{3}{2L} \left(-V_{pcc}^2 + u_P \right) - \omega Q - P \frac{R}{L} \\ \frac{dQ}{dt} &= \frac{3}{2L} u_Q - \omega Q - P \frac{R}{L} \end{aligned} \quad (11)$$

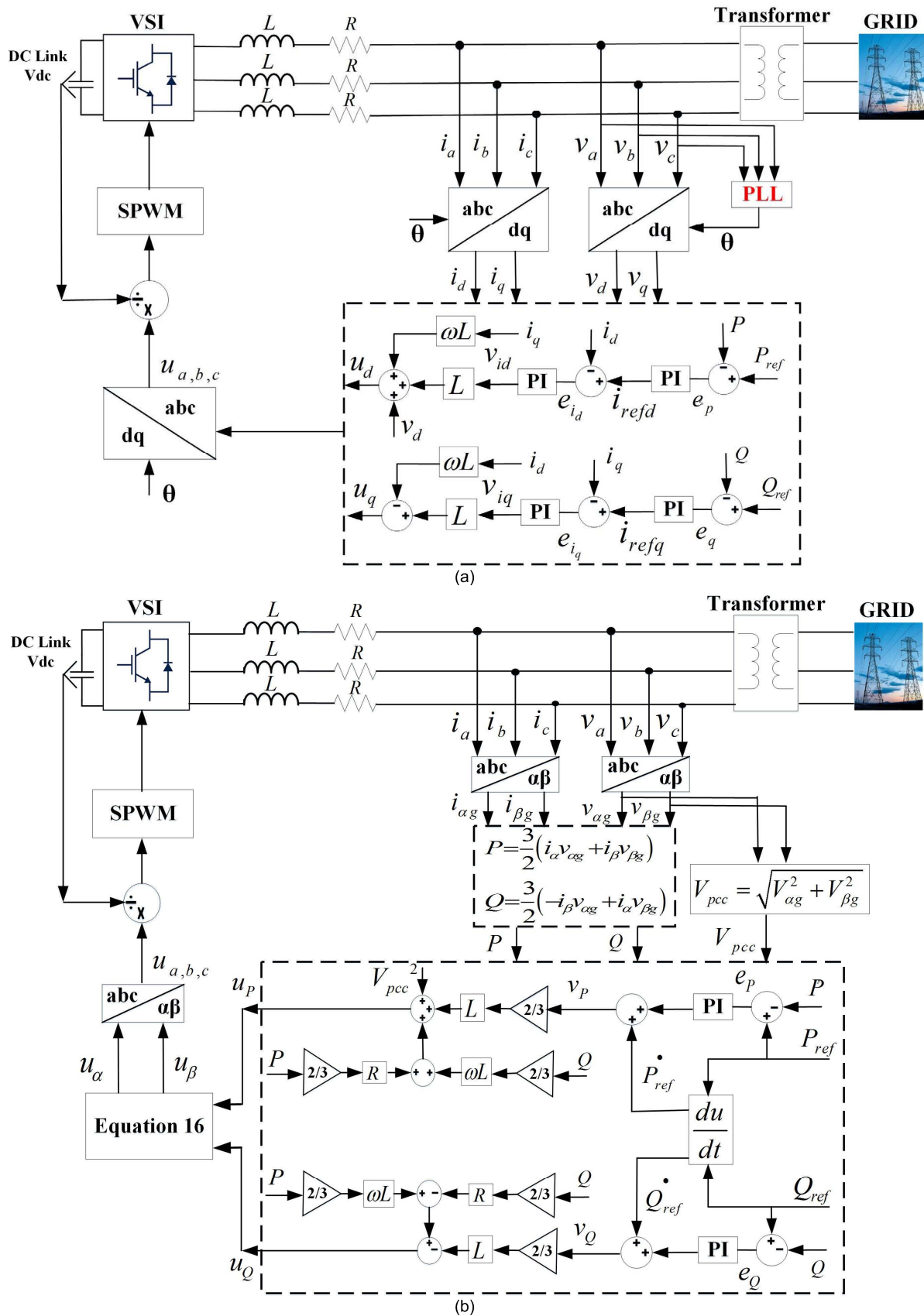


FIGURE 2. Representation of grid-connected MG's (a) conventional PLL-CCT based power controller [1], and (b) proposed PVMT-DPC method without PLL system.

IV. CONTROLLER DESIGN

A. DIRECT POWER CONTROL STRATEGY

To ensure stable and flexible operation of the new VSI model based on PVMT in (11), a robust and simple control method consisting of feedforward and feedback controllers is presented in this section. In Fig. 2, diagram of the PVMT-DPC method proposed for the PV VSI is displayed. Two PI controllers are used in this method, to track the reference real and reactive powers by governing their actual values.

By using (12), real and reactive power errors (e_p and e_q) can be calculated.

$$\begin{aligned} e_p &: = P_{ref} - P \\ e_q &: = Q_{ref} - Q \end{aligned} \tag{12}$$

where, P_{ref} & Q_{ref} are reference real & reactive power respectively. e_p and e_q are real and reactive power errors.

To eliminate the existed in the new MIMO system (11), a feedback and feed-forward based controller is designed which are as follows:

$$\begin{aligned} u_p &= \frac{2}{3}Lv_p + \frac{2}{3}L\omega Q + \frac{2}{3}RP + V_{pcc}^2 \\ u_q &= -\frac{2}{3}Lv_q - \frac{2}{3}RQ + \frac{2}{3}L\omega P \end{aligned} \tag{13}$$

where, v_p and v_q are feedback controller inputs and these can be obtained by means of (14).

$$\begin{aligned} v_p &= e_p K_{P,p} + K_{P,i} \int_0^t e_p(\tau) d\tau + \dot{P}_{ref} \\ v_q &= e_q K_{Q,p} + K_{Q,i} \int_0^t e_q(\tau) d\tau + \dot{Q}_{ref} \end{aligned} \tag{14}$$

where, $K_{P,p}$, $K_{P,i}$, $K_{Q,p}$, and $K_{Q,i}$ are gains of PI controllers to maintain steady state error to zero. The tuning method of these gains are presented in later section and their values are tabulated in Table 2.

The error dynamics of e_p and e_q can be obtained by substituting (13) and (14) in (11).

$$\begin{aligned} \dot{e}_p &= -K_{P,p} \int_0^t e_p(\tau) d\tau - e_p K_{P,p} \\ \dot{e}_q &= -K_{Q,p} \int_0^t e_q(\tau) d\tau - e_q K_{Q,p} \end{aligned} \tag{15}$$

Original control inputs (u_α and u_β) are obtained using (16).

$$\begin{aligned} u_\alpha &= \frac{-u_q v_{\beta g} + u_p v_{\alpha g}}{V_{pcc}^2} \\ u_\beta &= \frac{u_p v_{\beta g} + u_q v_{\alpha g}}{V_{pcc}^2} \end{aligned} \tag{16}$$

To generate switching signals for the switches of the via sinusoidal pulse width modulation (SPWM), 3-ph reference control signals are obtained by converting the control inputs of (16) using $\alpha\beta$ -abc transformation.

TABLE 2. Values of PI controllers' gains.

| PVMT-DPC method (PV VSI) | |
|--|---------|
| $K_{p,p}$ | 0.08 |
| $K_{p,q}$ | 0.0094 |
| $K_{i,p}$ | 0.0088 |
| $K_{i,q}$ | 0.032 |
| PLL-CCT based power control method (PV VSI) | |
| $K_{p,q}$ | 0.005 |
| $K_{id,p}$ | 1.03 |
| $K_{p,p}$ | 0.0001 |
| $K_{iq,p}$ | 0.256 |
| $K_{i,p}$ | 0.03 |
| $K_{i,q}$ | 0.06 |
| $K_{id,i}$ | 0.0008 |
| $K_{iq,i}$ | 0.001 |
| PLL-CCT based power control method (Battery VSI) | |
| $K_{p,qB}$ | 0.13 |
| $K_{p,pB}$ | 10000 |
| $K_{i,qB}$ | 3.01 |
| $K_{i,pB}$ | 0.00089 |
| $K_{p,idB}$ | 35 |
| $K_{p,iqB}$ | 0.07 |
| $K_{i,idB}$ | 600 |
| $K_{i,iqB}$ | 5 |
| Voltage Controller for DC link | |
| $K_{i,dc}$ | 2.5 |
| $K_{p,dc}$ | 50 |

B. DESIGN OF ROBUST CONTROL

The error dynamics of (15) can be denoted as (17) by defining $\dot{\psi}_p = e_p$ and $\dot{\psi}_q = e_q$.

$$\begin{aligned} \begin{bmatrix} \dot{e}_p \\ \dot{\psi}_p \\ \dot{e}_q \\ \dot{\psi}_q \end{bmatrix} &= \begin{bmatrix} -K_{P,p} & -K_{P,i} & 0 & 0 \\ 1 & 0 & 0 & 0 \\ 0 & 0 & -K_{Q,p} & -K_{Q,i} \\ 0 & 0 & 1 & 0 \end{bmatrix} \begin{bmatrix} e_p \\ \psi_p \\ e_q \\ \psi_q \end{bmatrix} \tag{17} \\ \begin{matrix} \leftarrow & \leftarrow & \leftarrow & \leftarrow & \leftarrow \\ \dot{x} & & A & & x \end{matrix} \end{aligned}$$

Parameter uncertainties, measurement noises and discretization errors cannot affect (17) during practical operation.

1) ASSUMPTION 1

Let, consider (11) as linear time invariant MIMO system in which uncertainties δ_p , δ_q and Δ are existed in such a way that

$$\begin{aligned} \dot{x} &= f_a(x, u_p, u_q, \delta_p, \delta_q) \\ &= \begin{bmatrix} \frac{3}{2L} (-V_{PCC}^2 + u_p) - \omega x_2 - x_1 \frac{R}{L} + \delta_p \\ \frac{3}{2L} u_q - \omega x_1 - x_2 \frac{R}{L} + \delta_q \end{bmatrix} \end{aligned} \tag{18}$$

where, δ_Q, δ_P confined as $0 \leq |\delta_Q| \leq \Delta, 0 \leq |\delta_P| \leq \Delta$. Parameter uncertainty in VSI relies on grid voltage/ frequency/ inductance. It is obvious, for a given operating point, the upper bound of uncertainty Δ needs to be estimated. Further, the VSI system's operating point exponential stability is always guaranteed by control law (13) with (14) and due to model parameter uncertainty, any DC offset is compensated by integral action. Thus, without loss of generality Assumption 1 is reasonable.

2) SUGGESTION 1

For new MIMO system (11), let consider a control law such that

$$\begin{aligned}\hat{v}_P &= K_{P,i} \int_0^t e_P(\tau) d\tau + e_P K_{P,p} + K_P \operatorname{sgn}(e_P) + \dot{P}_{ref} \\ \hat{v}_Q &= K_{Q,i} \int_0^t e_Q(\tau) d\tau + e_Q K_{Q,p} + K_Q \operatorname{sgn}(e_Q) + \dot{Q}_{ref}\end{aligned}\quad (19)$$

where, $K_P > \Delta$ and $K_Q > \Delta$, then the closed-loop system is also exponentially stable.

3) PROOF

When $\delta_p = 0$ and $\delta_Q = 0$, the closed-loop system is exponentially stable based on (17). When $\delta_p \neq 0$ and $\delta_Q \neq 0$, for simplicity in this study the terms δ_p and δ_Q are just considered. Consider a Lyapunov function such as

$$V = \frac{1}{2} e_P^2 + \frac{1}{2} e_Q^2 \quad (20)$$

By using (21), the time derivative of (20) could be found.

$$\dot{V} = e_Q (\delta_Q - K_Q \operatorname{sgn}(e_Q)) + e_P (\delta_P - K_P \operatorname{sgn}(e_P)) \quad (21)$$

If $K_P > \Delta$ and $K_Q > \Delta$ are considered as controller gains, then

$$\dot{V} \leq -K_{\Delta Q} |e_Q| - K_{\Delta P} |e_P| \quad (22)$$

where, $K_{\Delta Q} = K_Q - \Delta$ and $K_{\Delta P} = K_P - \Delta$.

C. DC LINK VOLTAGE CONTROLLER

During instabilities or disturbances to keep DC-link voltage constant, a DC-link voltage controller is used in this study which is shown in Fig. 3.

By using (23), DC-link voltage error can be expressed.

$$V_{dc_error} = (V_{dc}^*)^2 - (V_{dc})^2 \quad (23)$$

where, V_{dc}^* is the reference value of V_{dc} .

This DC-link error is fed to the PI controller to generate the reference DC current I_{dc_ref} to maintain a constant voltage at DC bus.

DC current reference I_{dc_ref} can be obtained using (24).

$$I_{dc_ref} = K_{p,dc} V_{dc_error} + K_{i,dc} \int_0^t V_{dc_error} dt \quad (24)$$

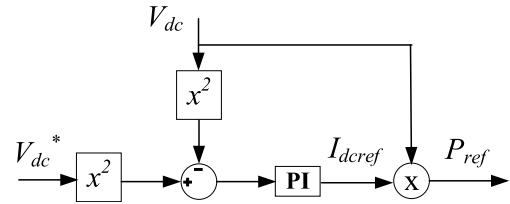


FIGURE 3. Schematic of controller for DC-link voltage.

where, the controller gains are $K_{p,dc}$ and $K_{i,dc}$ and the values are given in Table 2.

D. TUNING OF PI CONTROLLERS GAIN

A closed-loop system (25) can be obtained to design the PI controllers gain by substituting (12) to (14) into (11).

$$\begin{aligned}\frac{dP}{dt} &= -P \frac{R}{L} + K_{P,p} (P_{ref} - P) + K_{P,i} \int (P_{ref} - P) dt \\ \frac{dQ}{dt} &= -Q \frac{R}{L} + K_{Q,p} (Q_{ref} - Q) + K_{Q,i} \int (Q_{ref} - Q) dt\end{aligned}\quad (25)$$

By differentiating (25) a second-order system (26) can be obtained.

$$\begin{aligned}\frac{d^2P}{dt^2} &= -\frac{dP}{dt} \frac{R}{L} + K_{P,p} \frac{d}{dt} (P_{ref} - P) + K_{P,i} (P_{ref} - P) \\ \frac{d^2Q}{dt^2} &= -\frac{dQ}{dt} \frac{R}{L} + K_{Q,p} \frac{d}{dt} (Q_{ref} - Q) + K_{Q,i} (Q_{ref} - Q)\end{aligned}\quad (26)$$

Applying the Laplace transform to (26) results in

$$\begin{aligned}Ps^2 &= -sP \frac{R}{L} + sK_{P,p} (P_{ref} - P) + K_{P,i} (P_{ref} - P) \\ Qs^2 &= -sQ \frac{R}{L} + sK_{Q,p} (Q_{ref} - Q) + K_{Q,i} (Q_{ref} - Q)\end{aligned}\quad (27)$$

Using (27), PI controller gains could be can be selected.

By considering the overall system dynamics, the tuning of the gains of the PI controller for the proposed PVMT-DPC method is conducted. The values are calculated using phase margin (PM) and corner frequency (ω_{co}) of the VSI. The relationship between and corner frequency PM can be expressed as (28) [35].

$$PM = \prod / 2 - \omega_{co} (1.5T_s) \quad (28)$$

where, T_s is sampling period.

The proportional gain K_p can be calculated by using the cutoff frequency value obtained from (28).

$$K_p \approx \omega_{co} L \quad (29)$$

To abate PI regulator's phase contribution at corner frequency, during integral gain K_i calculation corner frequency is set one tenth (1/10) of ω_{co} [35]. Hence, K_i can be expressed as:

$$K_i = \frac{\omega_{co}}{10} K_p \quad (30)$$

V. RESULTS AND DISCUSSIONS

For a PV VSI of grid-tied MG, the proposed PLL less PVMT-DPC technique is implemented and the acquired results are presented in this section. The laboratory setup used in this study is represented in Fig. 4. On RTDS the real-time simulations are executed, which uses a PB5 processor card mounted on a rack, to facilitate the execution of the proposed grid-tied AC MG PV VSI power controller.



FIGURE 4. Proposed AC MG's PV VSI controller laboratory setup.

To verify the performance of the proposed PVMT-DPC technique, three case studies are taken into account. Initially, by varying references of real and reactive power, steady-state and reference power tracking performances of the proposed controller on a grid-connected PV VSI are justified in first & second case studies and the results are compared with the traditional PLL-CCT based control technique presented in [1]. In third case study, during MG's different operating states, solar irradiation and loads are changed to verify the proposed PV VSI controller performance integrated in an AC MG. Finally, to demonstrate the supremacy of the proposed PVMT-DPC technique a comparative analysis is presented in the third case study.

A. CASE 1: PERFORMANCE ANALYSIS OF PROPOSED PVMT-DPC METHOD FOR PV VSI CONNECTED TO GRID BY CHANGING REFERENCES OF BOTH REAL AND REACTIVE POWERS

The reference power tracking and steady-state performances of the proposed PVMT-DPC technique are represented in this section by varying both real and reactive power references and the performance is compared with conventional PLL-CCT based control technique.

1) ANALYSIS OF REFERENCE POWER TRACKING PERFORMANCE

Different real and reactive power references are set to test the power tracking performance of PVMT-DPC technique, by varying references of real and reactive powers from 0 MW to 0.1 MW (since PV output power is non-linear) and 0 MVar to 0.02 MVar respectively. It is seen from Fig. 5 (a) that after 1s the initial real power reference that is set to 0 MW is went upto 0.05 MW, later again it went further upto 0.1 MW at 3s and finally the power reference reduced to 0 MW at 5 s. The real power output of PV VSI controlled by the PVMT-DPC technique accurately traces the reference real powers

during different time intervals. Though from Fig. 5 (b) it can be seen that conventional PLL-CCT based power controller is able to track the reference powers, however, it is seen from the zoomed portion that PLL-CCT based power control technique's tracking speed (0.23 s) is 0.175 s slower than the tracking speed of proposed PVMT-DPC technique (0.055 s). Similarly, the reference power for the reactive power is also kept to 0 MVar initially. Then at 1 s and 3 s, it raised to 0.01 MVar and 0.02 MVar respectively and finally at 5 s, reference reactive power has reduced to 0 MVar. Controlled by PVMT-DPC technique the PV VSI output reactive power is following the reference reactive power accurately which is observed from Fig. 6 (a). On contrary, PLL-CCT based power controller is also able to track the reference reactive powers as shown in Fig. 6 (b). However, PVMT-DPC technique has shown faster tracking speed than that of PLL-CCT power controller. The required time to reach steady-state by the proposed PVMT-DPC technique is 3.03 s where PLL-CCT based power controller tracks it at 3.21 s and comparing both results the proposed controllers tracking speed is found 0.18 s faster than PLL-CCT based power controller.

2) ANALYSIS OF STEADY-STATE PERFORMANCE

In the steady state, the presence of power ripple is the main deterrent of the typical PLL-CCT based power controller. However, the issue is overcome by the proposed PVMT-DPC technique because the proposed controller has acquired decoupled LTI error dynamic, which is exponentially stable. The power ripples for both real and reactive powers are presented in Fig. 7 and 8 respectively which indicate that power ripples are have been highly mitigated through the implementation of PVMT-CCT technique compared to the typical PLL-CCT based power controller. For investigating the power ripples in both real and reactive power, 2.88 - 5 s is the appraised timespan. For the proposed PVMT-DPC method, it is observed from Fig. 7 (a) that in real power, there is very small ripple existed. However, large power ripple is observed for the traditional PLL-CCT based controller, which ranges from 0.0984 MW to 0.1006 MW and as seen from Fig. 7 (b), the actual real power is also not following the reference accurately. For reactive power also, large ripples are observed ranging from 0.019 MVar to 0.0208 MVar for the PLL-CCT based power controller, which can be seen from Fig. 8(b). On contrary, for the proposed PVMT-DPC technique as shown in Fig. 8 (a) like real power, reactive power also has very low ripple. In Fig. 9 for both the controllers, the PV VSI output current waveforms are depicted. The PV VSI output current for PVMT-DPC technique is pure sinusoidal in shape and has negligible noises, which can be seen from Fig. 9 (a). However, in Fig. 9 (b) large distortion is observed at PV VSI output current for PLL-CCT based power controller, even though current waveforms have sinusoidal shape. Further, it can be seen from Fig. 10 that according to IEC standard, the THD of PV VSI currents for the controllers are less than 5% [36]; however, current THD (1.697%) for

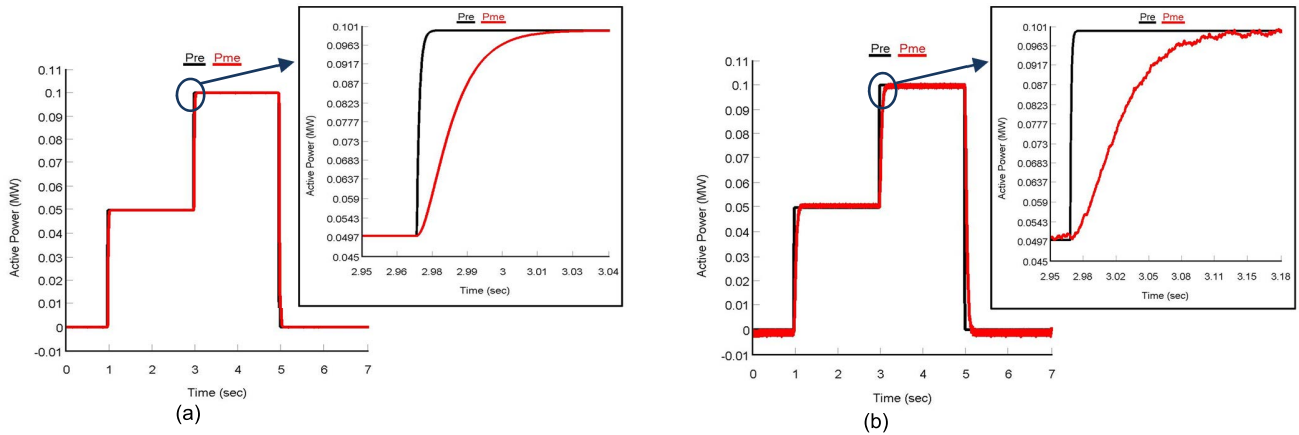


FIGURE 5. Tracking performance of real power for (a) PVMT-DPC technique and (b) PLL-CCT based controller [1].

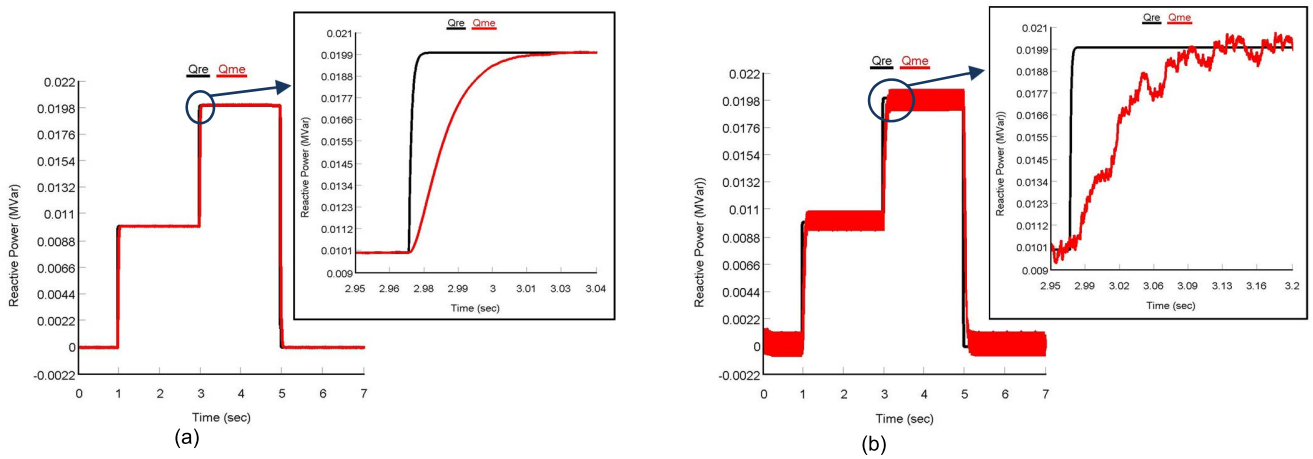


FIGURE 6. Tracking performance of reactive power for (a) PVMT-DPC technique and (b) PLL-CCT based controller [1].

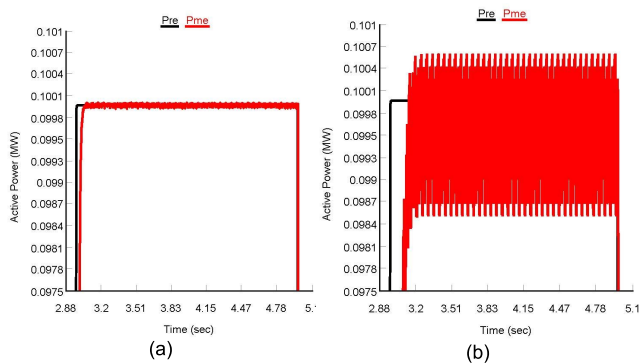


FIGURE 7. During steady-state ripples at real power for (a) PVMT-DPC technique and (b) PLL-CCT based controller [1].

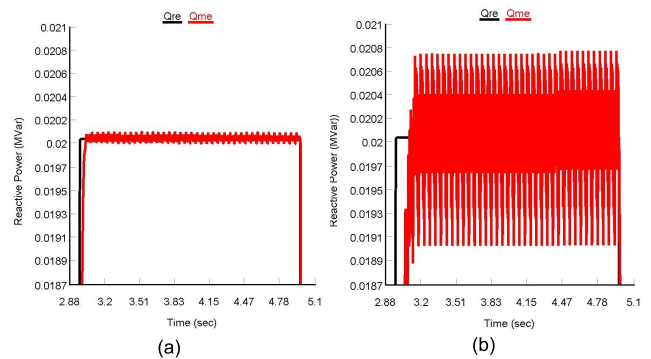


FIGURE 8. During steady-state ripples at reactive power for (a) PVMT-DPC technique and (b) PLL-CCT based controller [1].

PVMT-DPC technique is smaller than the THD (4.967%) obtained by PLL-CCT based power control technique. Therefore, it is certain that when PLL less PVMT-DPC is employed to control PV VSI, power ripples are very low compared to the traditional PLL-CCT based power control technique.

B. CASE 2: PERFORMANCE ANALYSIS OF PROPOSED PVMT-DPC METHOD FOR PV VSI CONNECTED TO GRID BY CHANGING REAL POWER REFERENCE WHILE REACTIVE POWER REFERENCE IS ZERO

When real power references are varied while reactive power reference is kept to zero, the results related to MG's PV

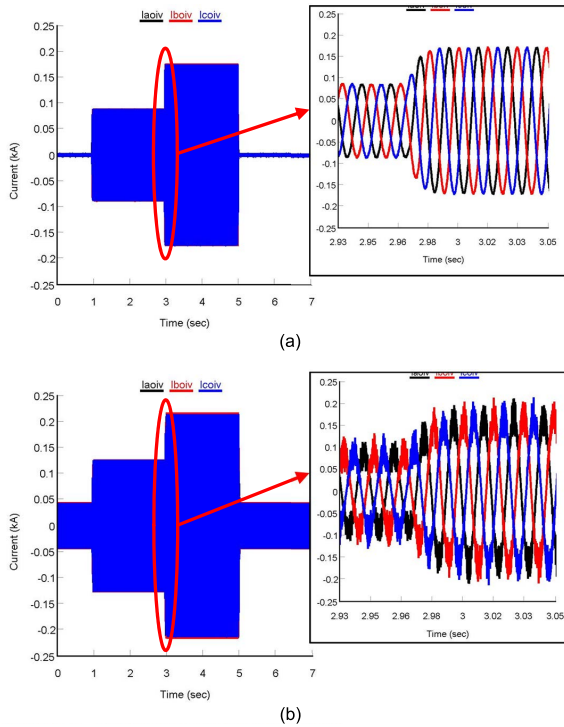


FIGURE 9. Output current of VSI for (a) PVMT-DPC technique and (b) PLL-CCT based controller [1].

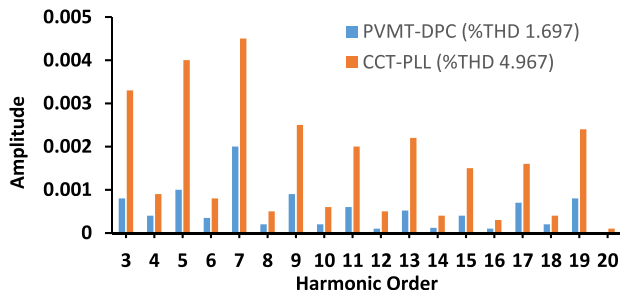


FIGURE 10. THD of inverter output current for PVMT-DPC method and PLL-CCT based power controller [1].

VSI output power and current are presented in this section to analyze the tracking and steady-state performances of the proposed PVMT-DPC technique.

1) ANALYSIS OF REFERENCE POWER TRACKING PERFORMANCE

For verifying proposed controller's tracking performance, different references of real power are set which varies from 0 MW to 0.1 MW similar to case 1, while references of reactive power for this case are not varied i.e. kept to 0 MVar. PV VSI output real power controlled by the proposed PVMT-DPC is tracking different reference real powers faster, flexibly and precisely as observed From Fig. 11 (a). On the other hand, although traditional PLL-CCT based power controller is also tracking the reference powers which can be seen from Fig. 11 (b), however, the tracking speed of this method is

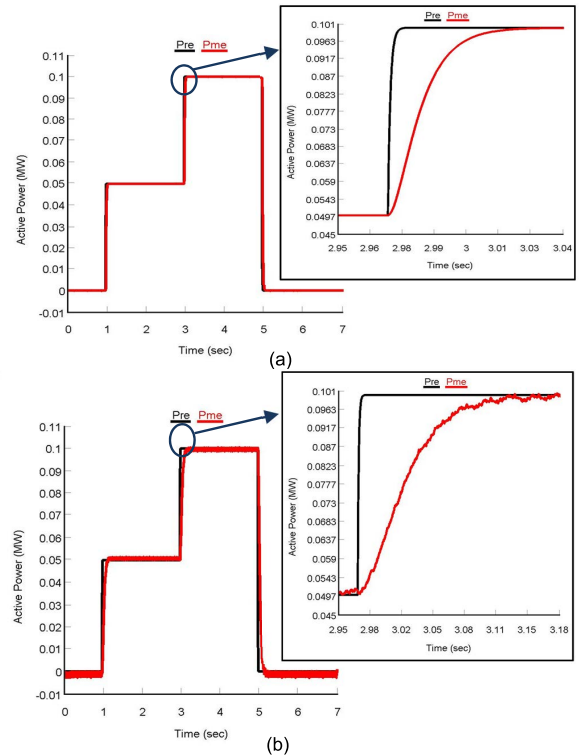


FIGURE 11. Tracking performance of real power for (a) PVMT-DPC technique and (b) PLL-CCT based controller [1].

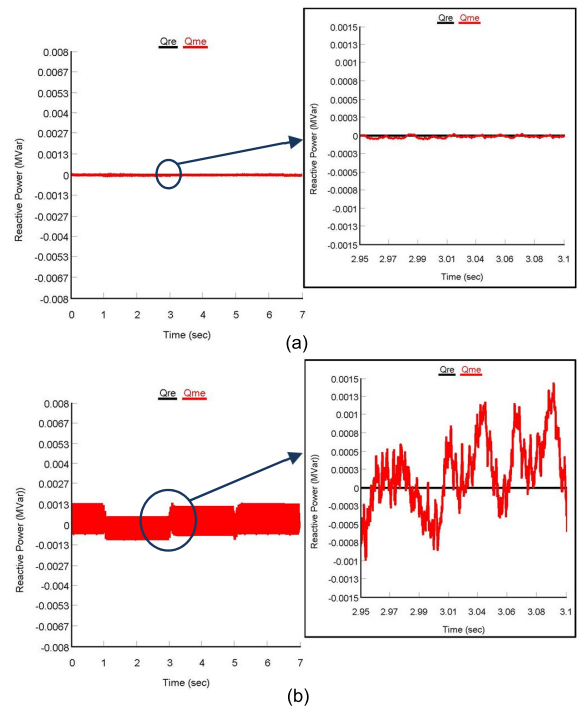


FIGURE 12. Tracking performance of reactive power for (a) PVMT-DPC technique and (b) PLL-CCT based controller [1].

0.23 s which is slower than the proposed PVMT-DPC method whose reference power tracking speed is 0.055 s. The PV VSI output reactive power controlled by PVMT-DPC technique

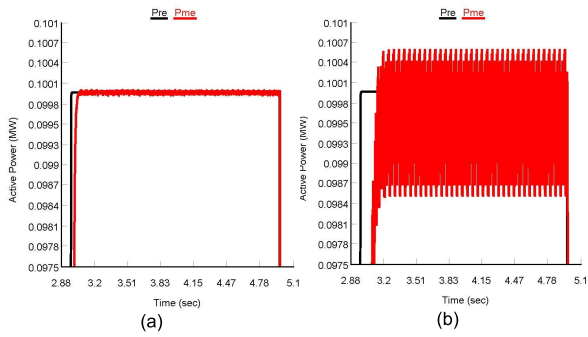


FIGURE 13. During steady-state ripples at real power for (a) PVMT-DPC technique and (b) PLL-CCT based controller [1].

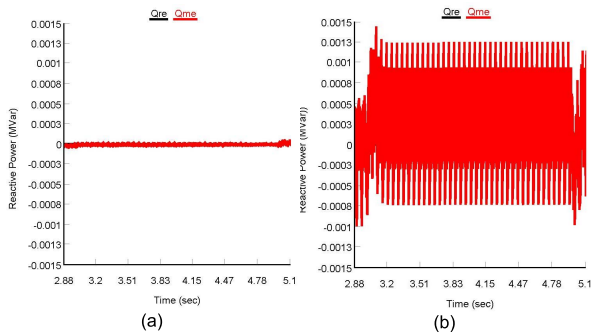


FIGURE 14. During steady-state ripples at reactive power for (a) PVMT-DPC technique and (b) PLL-CCT based controller [1].

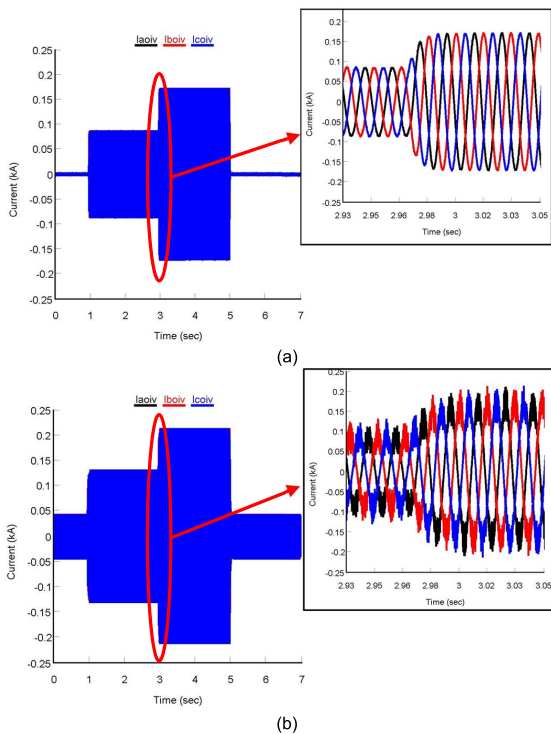


FIGURE 15. Output current of VSI for (a) PVMT-DPC technique and (b) PLL-CCT based controller [1].

for reactive power is also following the reference reactive power precisely as shown in Fig. 12 (a) at different time intervals which is set to 0 MVar. In addition, in PV VSI

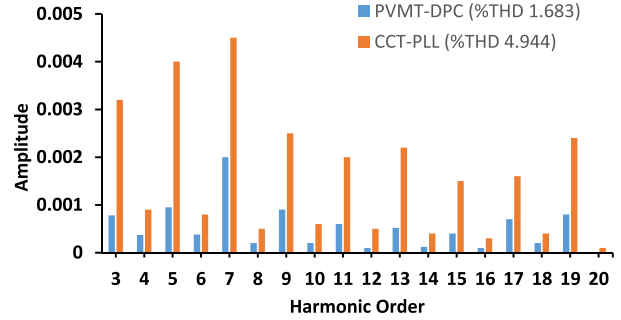


FIGURE 16. THD of inverter output current for PVMT-DPC method and PLL-CCT based power controller [1].

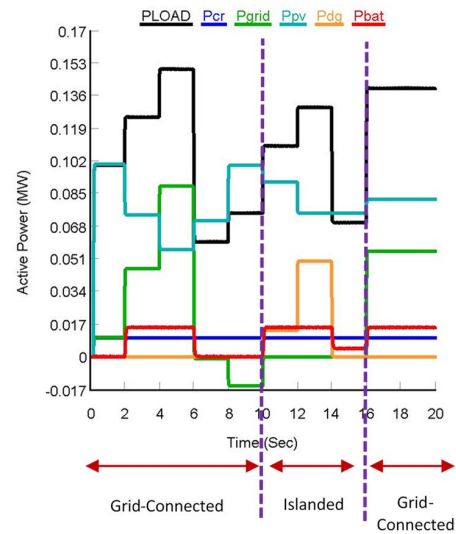


FIGURE 17. Active power flow in the MG during different operating modes.

output reactive power at different time intervals no overshoot and ripples are noticed for the proposed PVMT-DPC. On the other hand, as shown in Fig. 12 (b), there are large ripples and overshoots observed at the output of the PV VSI controlled PLL-CCT based controller, though it is able to track the reference reactive powers.

2) ANALYSIS OF STEADY-STATE PERFORMANCE

To inspect the ripples in reactive and real power for steady-state analysis, the time range considered is 2.88 – 5 s. For PVMT-DPC technique it is observed from Fig. 13 (a) that in VSI real power output, there is very low ripple occurred. However, as seen from Fig. 13 (b), for the PLL-CCT based controller, the output power is not following the reference precisely and it has also very large power ripples which fluctuates from 0.0984 MW to 0.1006 MW. Furthermore, as shown in Fig. 14 (b), the ripple is very high for the PLL-CCT based controller for reactive power and it is ranging from -0.001 MVar to 0.0015 MVar. contrary, as shown in Fig. 14 (a), reactive power has very low ripple almost null for PVMT-DPC technique. As depicted in Fig. 15, the VSI output current for PVMT-DPC technique has negligible distortion compared to PLL-CCT based controller. From Fig. 16 it can also be seen that for PVMT-DPC technique, THD of VSI

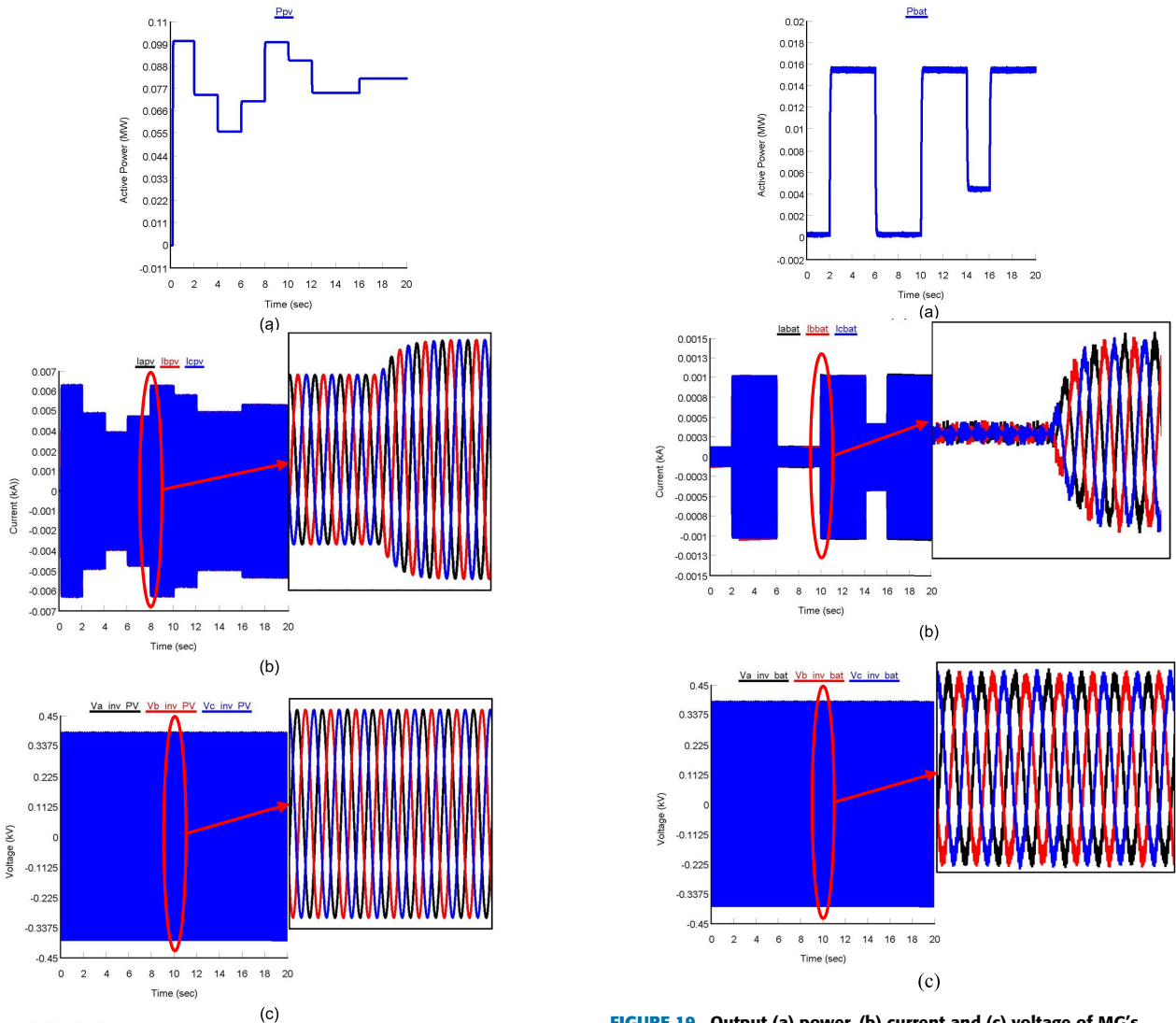


FIGURE 18. Output (a) power, (b) current and (c) voltage of MG's PV VSI.

output current is observed 1.683 % which is better than PLL-CCT based control technique's current THD (4.944 %).

C. CASE 3: PERFORMANCE ANALYSIS OF THE PROPOSED PVMT-DPC METHOD FOR PV VSI INTEGRATED WITH AC MG

Making sure the required power is flowing between MG and utility grid without discontinuing power supply to the load is vital role of grid-tied MG power controller. Additionally, in situations like fluctuating weather conditions and load demand, the VSI controller should also be capable of functioning accurately, flexibly and stable. By varying load demand and solar irradiation simultaneously in this section, the performance of the PV VSI with the proposed PVMT-DPC technique integrated with AC MG is validated to verify these real world situations. This section intends to verify whether during MG's different operating modes, the proposed controller can ensure necessary power flow between grid and MG accurately. Therefore, in this case, performance

FIGURE 19. Output (a) power, (b) current and (c) voltage of MG's battery VSI.

of the proposed PV VSI controller is not compared while discussing the results. However, in the following section, to show the preeminence of the proposed PVMT-DPC technique over other existed power control techniques of MG for grid-tied PV VSIs, a comparison is presented. Fig. 17 depicts the real-time simulation results for real power flow in AC MG's loads from different sources during MG's different operating modes and in Table 3, a summary of the power flow is presented.

It is seen from the results presented in Table 3 that during MG's different operating modes, the power flow is controlled easily by the power management system applied from [1] from different sources of MG to the load as well as to the utility grid. In addition, the proposed PVMT-DPC technique also shows excellent performance during the transition from islanded to grid reconnected mode and vice versa by controlling the power flow proficiently.

With the proposed PVMT-DPC technique during grid resynchronization no disturbance in the PV VSI power has

TABLE 3. Summary of power flow in AC MG.

| Time (s) | Variables | | Load Demand | | Power Generation | | | |
|----------|---------------------------------------|-----------------|-------------------------------------|---|---|-------------------------------------|---|--|
| | Solar Irradiation (W/m ²) | Total Load (MW) | Load Critical, P _{cr} (MW) | Load Non-critical, P _{Load} (MW) | Power from grid, P _{grid} (MW) | Power from PV, P _{pv} (MW) | Power from Diesel Generator, P _{dg} (MW) | Power from Battery P _{bat} (MW) |
| 0 to2 | 1000 (initial) | 0.1 (initial) | 0.01 | 0.1 | 0.01 | 0.1 | 0 | 0 |
| 2 to4 | 800 | 0.135 | 0.01 | 0.125 | 0.046 | 0.074 | 0 | 0.015 |
| 4 to6 | 600 | 0.16 | 0.01 | 0.15 | 0.089 | 0.056 | 0 | 0.015 |
| 6 to8 | 750 | 0.07 | 0.01 | 0.06 | -0.001 | 0.071 | 0 | 0 |
| 8 to10 | 1000 | 0.085 | 0.01 | 0.075 | -0.015 | 0.1 | 0 | 0 |
| 10 to12 | 950 | 0.12 | 0.01 | 0.11 | 0 | 0.091 | 0.014 | 0.015 |
| 12 to14 | 820 | 0.14 | 0.01 | 0.13 | 0 | 0.075 | 0.05 | 0.015 |
| 14 to16 | 820 | 0.08 | 0.01 | 0.07 | 0 | 0.075 | 0 | 0.005 |
| 16 to 20 | 870 | 0.145 | 0.01 | 0.135 | 0.05 | 0.08 | 0 | 0.015 |

TABLE 4. Comparison between proposed PVMT-DPC and conventional grid-tied MGs power controllers.

| # | Controller | Grid Synchronization | No. of control loops | Settling Time (s) | Percentage of ripples in Active Power (%) | VSI Output Current (%THD) | VSI Output Voltage (%THD) |
|----|------------|-------------------------------------|----------------------|-------------------|---|---------------------------|---------------------------|
| 1 | Proposed | Direct power calculation (PLL less) | 1 | 0.055 | 0.1 | 1.686 | 1.44 |
| 2 | Ref [1] | PLL | 2 | 0.23 | 6.2 | 4.975 | 3.91 |
| 3 | Ref [3] | PLL | 2 | 0.245 | 8.1 | 5.641 | 4.15 |
| 4 | Ref [4] | PLL | 2 | 0.225 | 5.9 | 4.967 | 3.85 |
| 5 | Ref [5] | PLL | 2 | 0.215 | 5.1 | 4.87 | 3.83 |
| 6 | Ref [7] | PLL | 2 | 0.15 | 3.6 | 3.95 | 2.59 |
| 7 | Ref [11] | PLL | 2 | 0.17 | 4 | 4.11 | 2.75 |
| 8 | Ref [14] | PLL | 2 | 0.22 | 4.3 | 4.76 | 3.80 |
| 9 | Ref [26] | PLL less Direct power calculation | 2 | 0.13 | 1.0 | 2.226 | 2.01 |
| 10 | Ref [23] | FLL | 2 | 0.15 | 2.2 | 3.17 | 2.56 |

been perceived. In addition, as the PV system is capable of supplying the power with respect to the solar irradiation changes, it is proved that the proposed PVMT-DPC technique has also performed efficiently to control power flow from PV.

The output power, current and voltage of PV and battery VSIs are presented respectively in Fig. 18 and 19. It is seen from Fig. 18 (a) that ripples in the output power for PV VSI is small and the PV VSI is also relinquishing precisely the power supplied by the PV. Furthermore, as the PVMT-DPC is implemented to control the PV inverter, hence, output current and voltage also have less distortion which are shown in Fig. 18 (b) and (c) respectively. On the other hand, the output power, current and voltage of battery VSI have high oscillations due to the use of conventional PLL-CCT

controller to control the battery VSI, which are presented in Fig. 19 (a), (b) and (c) respectively.

In Fig. 20 (a), (b), and (c), the THDs of PV and battery VSI output currents and voltages are depicted respectively. From the figures, it is seen that battery VSI is 4.718 % which is higher than that of PV VSI which is 1.686 %. As for voltages, also PV VSI voltage THD (1.44 %) is lower than battery voltage THD (2.592 %). Finally, in Figure 21 (a), (b) and (c) the corresponding grid power, current and voltage are presented respectively. It can be perceived that according to the demand of MG, grid is supplying or absorbing power to meet the load demand of MG. Further, grid current and voltage sustain 60 Hz frequency, have nominal contortion and are sinusoidal in shape.

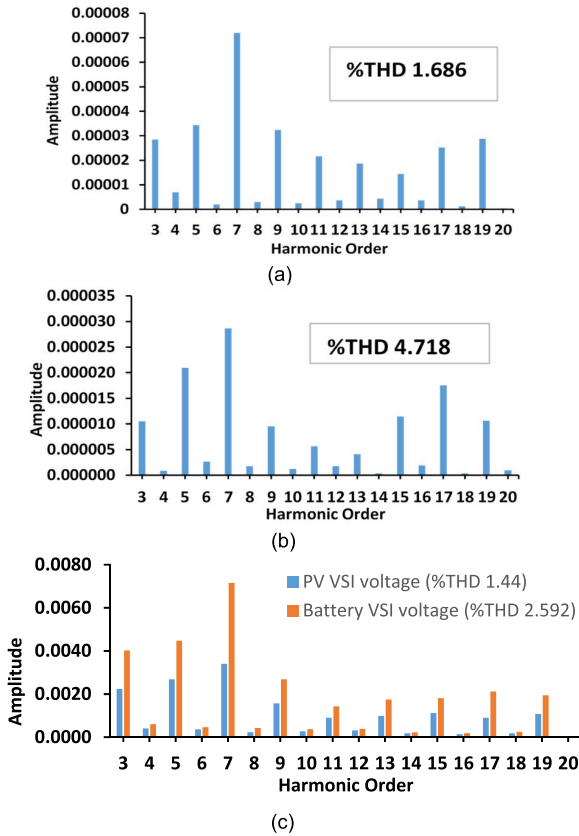


FIGURE 20. THD of output currents of (a) PV VSI, (b) Battery VSI and (c) output voltages of PV & battery VSIs.

D. PERFORMANCE COMPARISON AMONG PROPOSED PVMT-DPC METHOD AND EXISTING GRID-CONNECTED MG CONTROLLERS

In this part, the proposed PVMT-DPC approach performance is compared to the existing grid-tied MG power control systems [1], [3], [4], [5], [7], [11], [14], [23], [26]. All of these controllers are implemented in RTDS for the PV VSI shown in Figure 1. Real-time simulations are performed to acquire the results. To ensure a fair comparison can be obtained, all MG parameters were kept same across all controllers. The results of the comparative study, which was done on the basis of six indicators, are provided in Table 4. The comparison indicators are synchronization method, number of control loops, settling time, power ripple, output voltage of the inverter and THD of the current. It can be indicated in the Table that for grid-connected MG’s PV VSI, the proposed PVMT-DPC approach surpassed power controllers of the other grid-connected MG VSI for all of the performance analysis indicators. Fig. 19 depicts the AC MG operated in grid-tied mode, and all of the findings are displayed during the duration of 1-2 s. For example, the suggested PVMT-DPC technique settles faster than the controllers proposed in [1], [3], [4], [5], [7], [11], [14], [23], and [26] by 0.175 s, 0.19 s, 0.17 s, 0.16 s, 0.095 s, 0.115 s, 0.165 s, 0.075 s, and 0.085 s, respectively. Furthermore, the THD of the PV VSI output current is observed to be 1.686%, which is around

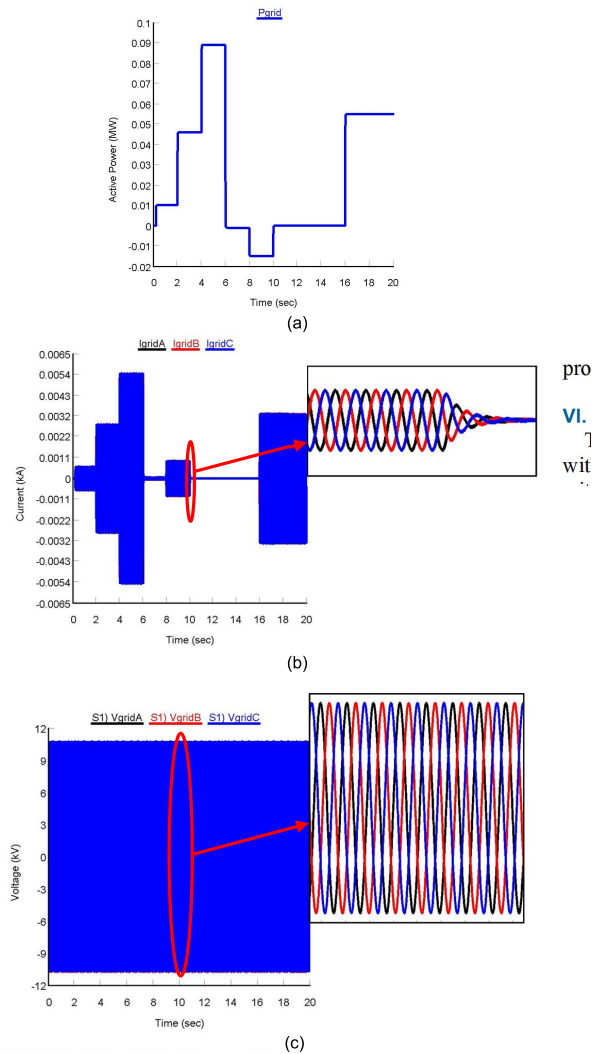


FIGURE 21. Utility grid’s (a) power, (b) current and (c) voltage.

ranges of 2.264% to 3.289% lesser than the controllers in [1], [3], [4], [5], [7], [11], [14], [23], and [26]. Furthermore, as contrasted to the PV VSIs output power ripples controlled by the controllers suggested in [1], [3], [4], [5], [7], [11], [14], [23], and [26], the ripple in the output power for the proposed PVMT-DPC is very low.

VI. CONCLUSION

This work has introduced a grid-tied MG’s PV VSI without establishing PLL system and Park transformation with PVWMT-based DPC. To verify the proposed power controller’s performance, CHIL simulations were run utilizing the RTDS power tool in real-time environment for three multiple cases: altering these two real and reactive power references, varying solely real power reference, and different AC MG working modes. Throughout all three cases, the performance of the proposed PVMT-DPC has been evaluated in comparison to that of conventional MG power controllers in order to demonstrate its effectiveness.

Real-time simulation results for case-1 and case-2 demonstrate that the proposed PVMT-DPC approach has high accuracy and flexibility in tracking both real and reactive power with respect to their reference powers. The proposed power controller has demonstrated improved dynamic performance during the transient state, as evidenced by its settling time of 0.055 s during the transient condition. The suggested PVMT-DPC controller shows no overshoot for the output reactive power of PV VSI and reaches steady state in a relatively short time (0.06 s). The output reactive power of the VSI for the power controller based on PLL-CCT based power controller, on the other hand, required roughly 0.23 s to achieve stability state. The suggested controller also performs well in steady-state, as the ripples in the PV VSI output power have been greatly decreased, and the THD of the VSI output current attained is 1.697%, which is far below the IEC standard of 5%. However, when compared to the suggested PVMT-DPC technique, the THD obtained using a traditional PLL-CCT based power controller is very high (4.967%). Furthermore, for case-3, various sources of MG, grid, and load power delivery operation during the grid-tied, islanded, and grid reconnected modes of the MG have proven that the developed controller performed admirably. The effect of maintaining the MG and grid power flow has caused the suggested PVMT-DPC approach to work admirably in grid-tied mode, according to the real-time simulation findings. Finally, to demonstrate the superiority of the proposed PVMT DPC approach, a comparative study with existing grid-tied MG power control methods has been performed. When it comes to PLL and FLL systems-based synchronization methods consisted of two control loops, for the factors such as power ripples, total harmonic distortion, and settling time, it has been discovered that the developed PVMT-DPC technique outperforms all existing controllers that use PLL and FLL.

This work validated the performance of the PLL less PVMT-DPC approach for grid-connected MG's VSI through real-time simulations during normal grid condition only. In future work, a laboratory prototype will be developed to verify the performance of the proposed controller to show prove its real world feasibility for both normal and weak grid conditions.

REFERENCES

- [1] S. Ahmad, S. Mekhilef, and H. Mokhlis, "DQ-axis synchronous reference frame based P-Q control of grid connected AC microgrid," in *Proc. IEEE Int. Conf. Comput., Power Commun. Technol. (GUCON)*, Oct. 2020, pp. 842–847.
- [2] M. A. Hossain, H. R. Pota, M. J. Hossain, and F. Blaabjerg, "Evolution of microgrids with converter-interfaced generations: Challenges and opportunities," *Int. J. Electr. Power Energy Syst.*, vol. 109, pp. 160–186, Jul. 2019.
- [3] M. Worku, M. Hassan, and M. Abido, "Real time energy management and control of renewable energy based microgrid in grid connected and island modes," *Energies*, vol. 12, no. 2, p. 276, Jan. 2019.
- [4] A. Safa, E. L. M. Berkouk, Y. Messlem, and A. Gouichiche, "A robust control algorithm for a multifunctional grid tied inverter to enhance the power quality of a microgrid under unbalanced conditions," *Int. J. Electr. Power Energy Syst.*, vol. 100, pp. 253–264, Sep. 2018.
- [5] J. Kaushal and P. Basak, "Power quality control based on voltage sag/swell, unbalancing, frequency, THD and power factor using artificial neural network in PV integrated AC microgrid," *Sustain. Energy, Grids Netw.*, vol. 23, Sep. 2020, Art. no. 100365.
- [6] S. Adhikari, F. Li, and H. Li, "PQ and PV control of photovoltaic generators in distribution systems," *IEEE Trans. Smart Grid*, vol. 6, no. 6, pp. 2929–2941, Nov. 2015.
- [7] G. Lou, W. Gu, J. Zhu, P. Li, and X. Zhang, "A novel control strategy for the seamless transfer of microgrids based on disturbance observer," *Int. J. Electr. Power Energy Syst.*, vol. 118, Jun. 2020, Art. no. 105804.
- [8] I. Abadlia, M. Adjabi, and H. Bouzeria, "Sliding mode based power control of grid-connected photovoltaic-hydrogen hybrid system," *Int. J. Hydrogen Energy*, vol. 42, no. 47, pp. 28171–28182, Nov. 2017.
- [9] W. Al-Saedi, S. W. Lachowicz, D. Habibi, and O. Bass, "Power flow control in grid-connected microgrid operation using particle swarm optimization under variable load conditions," *Int. J. Electr. Power Energy Syst.*, vol. 49, pp. 76–85, Jul. 2013.
- [10] S. Adhikari and F. Li, "Coordinated V-f and P-Q control of solar photovoltaic generators with MPPT and battery storage in microgrids," *IEEE Trans. Smart Grid*, vol. 5, no. 3, pp. 1270–1281, May 2014.
- [11] S. Y. M. Mousavi, A. Jalilian, M. Savaghebi, and J. M. Guerrero, "Coordinated control of multifunctional inverters for voltage support and harmonic compensation in a grid-connected microgrid," *Electr. Power Syst. Res.*, vol. 155, pp. 254–264, Feb. 2018.
- [12] W. Feng, K. Sun, Y. Guan, J. M. Guerrero, and X. Xiao, "Active power quality improvement strategy for grid-connected microgrid based on hierarchical control," *IEEE Trans. Smart Grid*, vol. 9, no. 4, pp. 3486–3495, Jul. 2018.
- [13] R. Sedaghati and M. R. Shakarami, "A novel control strategy and power management of hybrid PV/FC/SC/battery renewable power system-based grid-connected microgrid," *Sustain. Cities Soc.*, vol. 44, pp. 830–843, Jan. 2019.
- [14] A. Guichi, S. Mekhilef, E. M. Berkouk, and A. Talha, "Optimal control of grid-connected microgrid PV-based source under partially shaded conditions," *Energy*, vol. 230, Sep. 2021, Art. no. 120649.
- [15] L. Lee, C. Liu, Y. Xu, K. P. Schneider, F. K. Tuffner, K. Mo, and D. T. Ton, "Dynamics and control of microgrids as a resiliency source," *Int. Trans. Electr. Energy Syst.*, vol. 30, no. 11, Nov. 2020, Art. no. e12610.
- [16] Z. Ali, N. Christofides, L. Hadjidemetriou, E. Kyriakides, Y. Yang, and F. Blaabjerg, "Three-phase phase-locked loop synchronization algorithms for grid-connected renewable energy systems: A review," *Renew. Sustain. Energy Rev.*, vol. 90, pp. 434–452, Jul. 2018.
- [17] S.-J. Lee, H. Kim, S.-K. Sul, and F. Blaabjerg, "A novel control algorithm for static series compensators by use of PQR instantaneous power theory," *IEEE Trans. Power Electron.*, vol. 19, no. 3, pp. 814–827, May 2004.
- [18] M. Davari and Y. A.-R. I. Mohamed, "Robust vector control of a very weak-grid-connected voltage-source converter considering the phase-locked loop dynamics," *IEEE Trans. Power Electron.*, vol. 32, no. 2, pp. 977–994, Feb. 2017.
- [19] X. Wang, L. Harnefors, and F. Blaabjerg, "Unified impedance model of grid-connected voltage-source converters," *IEEE Trans. Power Electron.*, vol. 33, no. 2, pp. 1775–1787, Feb. 2018.
- [20] X. Wang and F. Blaabjerg, "Harmonic stability in power electronic-based power systems: Concept, modeling, and analysis," *IEEE Trans. Smart Grid*, vol. 10, no. 3, pp. 2858–2870, May 2019.
- [21] L. Harnefors, X. Wang, A. G. Yepes, and F. Blaabjerg, "Passivity-based stability assessment of grid-connected VSCs—An overview," *IEEE J. Emerg. Sel. Topics Power Electron.*, vol. 4, no. 1, pp. 116–125, Mar. 2016.
- [22] B. Wen, D. Dong, D. Boroyevich, P. Mattavelli, R. Burgos, and Z. Shen, "Impedance-based analysis of grid-synchronization stability for three-phase paralleled converters," *IEEE Trans. Power Electron.*, vol. 31, no. 1, pp. 26–38, Jan. 2016.
- [23] S. Kewat and B. Singh, "Grid synchronization of WEC-PV-BES based distributed generation system using robust control strategy," *IEEE Trans. Ind. Appl.*, vol. 56, no. 6, pp. 7088–7098, Nov. 2020.
- [24] P. Rodríguez, A. Luna, I. Candela, R. Mujal, R. Teodorescu, and F. Blaabjerg, "Multiresonant frequency-locked loop for grid synchronization of power converters under distorted grid conditions," *IEEE Trans. Ind. Electron.*, vol. 58, no. 1, pp. 127–138, Jan. 2010.
- [25] P. Šimek, J. Škrámlík, and V. Valouch, "A frequency locked loop strategy for synchronization of inverters used in distributed energy sources," *Int. J. Electr. Power Energy Syst.*, vol. 107, pp. 120–130, May 2019.
- [26] S. Ahmad, S. Mekhilef, and H. Mokhlis, "An improved power control strategy for grid-connected hybrid microgrid without park transformation and phase-locked loop system," *Int. Trans. Electr. Energy Syst.*, vol. 31, no. 7, Jul. 2021, Art. no. e12922.
- [27] Y. Gui, X. Wang, and F. Blaabjerg, "Vector current control derived from direct power control for grid-connected inverters," *IEEE Trans. Power Electron.*, vol. 34, no. 9, pp. 9224–9235, Sep. 2019.

- [28] Y. Gui, C. Kim, C. C. Chung, J. M. Guerrero, Y. Guan, and J. C. Vasquez, "Improved direct power control for grid-connected voltage source converters," *IEEE Trans. Ind. Electron.*, vol. 65, no. 10, pp. 8041–8051, Oct. 2018.
- [29] D.-K. Choi and K.-B. Lee, "Dynamic performance improvement of AC/DC converter using model predictive direct power control with finite control set," *IEEE Trans. Ind. Electron.*, vol. 62, no. 2, pp. 757–767, Feb. 2015.
- [30] S. Vazquez, A. Marquez, R. Aguilera, D. Quevedo, J. I. Leon, and L. G. Franquelo, "Predictive optimal switching sequence direct power control for grid-connected power converters," *IEEE Trans. Trans. Ind. Electron.*, vol. 62, no. 4, pp. 2010–2020, Apr. 2015.
- [31] D. Çelik and M. E. Meral, "A coordinated virtual impedance control scheme for three phase four leg inverters of electric vehicle to grid (V2G)," *Energy*, vol. 246, May 2022, Art. no. 123354.
- [32] M. E. Meral and D. Çelik, "Mitigation of DC-link voltage oscillations to reduce size of DC-side capacitor and improve lifetime of power converter," *Electr. Power Syst. Res.*, vol. 194, May 2021, Art. no. 107048.
- [33] D. Çelik, "Lyapunov based harmonic compensation and charging with three phase shunt active power filter in electrical vehicle applications," *Int. J. Electr. Power Energy Syst.*, vol. 136, Mar. 2022, Art. no. 107564.
- [34] Y. Gao and Q. Ai, "Distributed cooperative optimal control architecture for AC microgrid with renewable generation and storage," *Int. J. Electr. Power Energy Syst.*, vol. 96, pp. 324–334, Mar. 2018.
- [35] Y. Gui, X. Wang, F. Blaabjerg, and D. Pan, "Control of grid-connected voltage-source converters: The relationship between direct-power control and vector-current control," *IEEE Ind. Electron. Mag.*, vol. 13, no. 2, pp. 31–40, Jun. 2019.
- [36] *Photovoltaic (PV) systems Characteristics of the Utility Interface*, Standard IEC 61727, 2004.



and artificial intelligence application in power systems.

SHAMEEM AHMAD was born in Chittagong, Bangladesh, in 1985. He received the B.E. degree in electrical and electronics engineering from Visveswararajah Technological University (VTU), Belgaum, India, in 2009, and the master's degree in electrical engineering from Universiti Malaya, Malaysia, in 2014, where he is currently pursuing the Ph.D. degree. His research interests include microgrid control and management, inverter control, FACTS controllers, power system stability,



UMME KULSUM JHUMA was born in Dhaka, Bangladesh, in 1995. She received the B.Sc. degree in electrical and electronics engineering from American International University Bangladesh, Dhaka, in 2017, and the master's degree in electrical engineering from Universiti Malaya, Malaysia, in 2022. Her research interests include microgrid control and management, smart grid, islanding detection of distributed generators, and inverter control.



School of Technology and Innovations, University of Vaasa, Finland. His current research interests include smart grid applications, wide-area monitoring, protection, control, distributed generation, power system stability, and frequency control.

MAZAHER KARIMI (Senior Member, IEEE) received the Ph.D. degree in electrical energy and power systems from the University of Malaya, Kuala Lumpur, Malaysia, in 2013. He worked as a Postdoctoral Research Fellow at the University of Malaya, from 2014 to 2015. He joined The University of Manchester as a Research Associate, from 2016 to 2017. From 2017 to 2020, he was an Assistant Professor at Gonbad Kavous University, Iran. He is currently an Assistant Professor at the



ALIREZA POURDARYAEI received the bachelor's degree in electrical and electronic engineering from Hormozgan University, Iran, in 2010, and the M.Eng.Sc. degree in industrial electronic and control and the Ph.D. degree in power systems from the University of Malaysia (UM), in 2014 and February 2020, respectively. His current research interests include distribution automation, artificial intelligence (AI), and energy management and forecasting.



more than 400 publications in academic journals and proceedings and five books with more than 29,000 citations. His research interests include power conversion techniques, control of power converters, maximum power point tracking (MPPT), renewable energy, energy efficiency, smart grid, microwave, and wireless technologies. He is a fellow of the Institution of Engineering and Technology (IET). He is frequently invited as an honorary keynote lecturers at international conferences, congress, meetings, and symposiums. He has been listed by the Thomson Reuters (Clarivate Analytics) as one of the Highly Cited (Hi.Ci.) engineering researchers in the world, and included in the "Thomson Reuters The World's Most Influential Scientific Minds: 2018, 2019, 2020, and 2021." He is an Associate Editor of various top journals, such as IEEE TRANSACTIONS ON POWER ELECTRONICS and the *Journal of Power Electronics*.

SAAD MEKHILEF (Fellow, IEEE) is a Chartered Engineer (C.Eng.). He is actively involved in industrial consultancy for major corporations in the Power Electronics and Renewable Energy Projects. He is an Honorary Professor at the Department of Electrical Engineering, University of Malaya. He is also a Distinguished Professor at the School of Science, Computing and Engineering Technologies, Swinburne University of Technology, Australia. He has authored and coauthored



power system resilience, smart grid, distribution automation, and power system protection. His outstanding research had been recognized by Stanford University, in 2020 as one of the top 2% of scientists in the world. In 2021, he was awarded Top Research Scientist Malaysia by Academic Science Malaysia.

HAZLIE MOKHLIS (Senior Member, IEEE) received the B.E. degree in electrical engineering in 1999, the M.Eng.Sc. degree from the Universiti Malaya (UM), Malaysia, in 2002, and the Ph.D. degree from The University of Manchester, U.K., in 2009. He is currently a Professor and leading the Power and Energy Systems Research Group, Department of Electrical Engineering, UM. He is an active researcher in the area of power and energy systems. His research interests include



special research interests include power system transient simulation, protection of power systems, grid integration of distributed generation, and microgrids.

KIMMO KAUHANIEMI (Member, IEEE) received the M.S. and Ph.D. degrees in electrical engineering from the Tampere University of Technology, Finland, in 1987 and 1993, respectively. Previously, he was employed at the ABB Corporate Research Center and the VTT Technical Research Centre of Finland. He is currently with the University of Vaasa, where he is currently a Professor of electrical engineering and also leads the Smart Electric Systems Research Group. His

...